

Electronic Supplementary Information

Pseudo-ordered distribution of Ir nanocrystals on h-BN

Antonio J. Martínez-Galera¹ and José M. Gómez-Rodríguez^{1,2,3}

¹ Departamento de Física de la Materia Condensada, Universidad Autónoma de Madrid, E-28049

Madrid, Spain

² Condensed Matter Physics Center (IFIMAC), Universidad Autónoma de Madrid, E-28049

Madrid, Spain

³ Instituto Nicolás Cabrera, Universidad Autónoma de Madrid, E-28049 Madrid, Spain

Ir deposition

As mentioned in the experimental section of the main manuscript, Ir was deposited by sublimation from a current heated wire. It was calibrated by means of STM imaging after deposition on pristine Ir(111) and Rh(111) surfaces. Figure S1a-c show STM images acquired after deposition of increasing amounts of Ir on an Ir(111) substrate. Likewise, Figure S1d-f displays the respective topographs acquired for the case of a Rh(111) support. In this case, Auger Electron Spectroscopy (AES) measurements confirming the presence of Ir on the substrate were also performed (see next section).

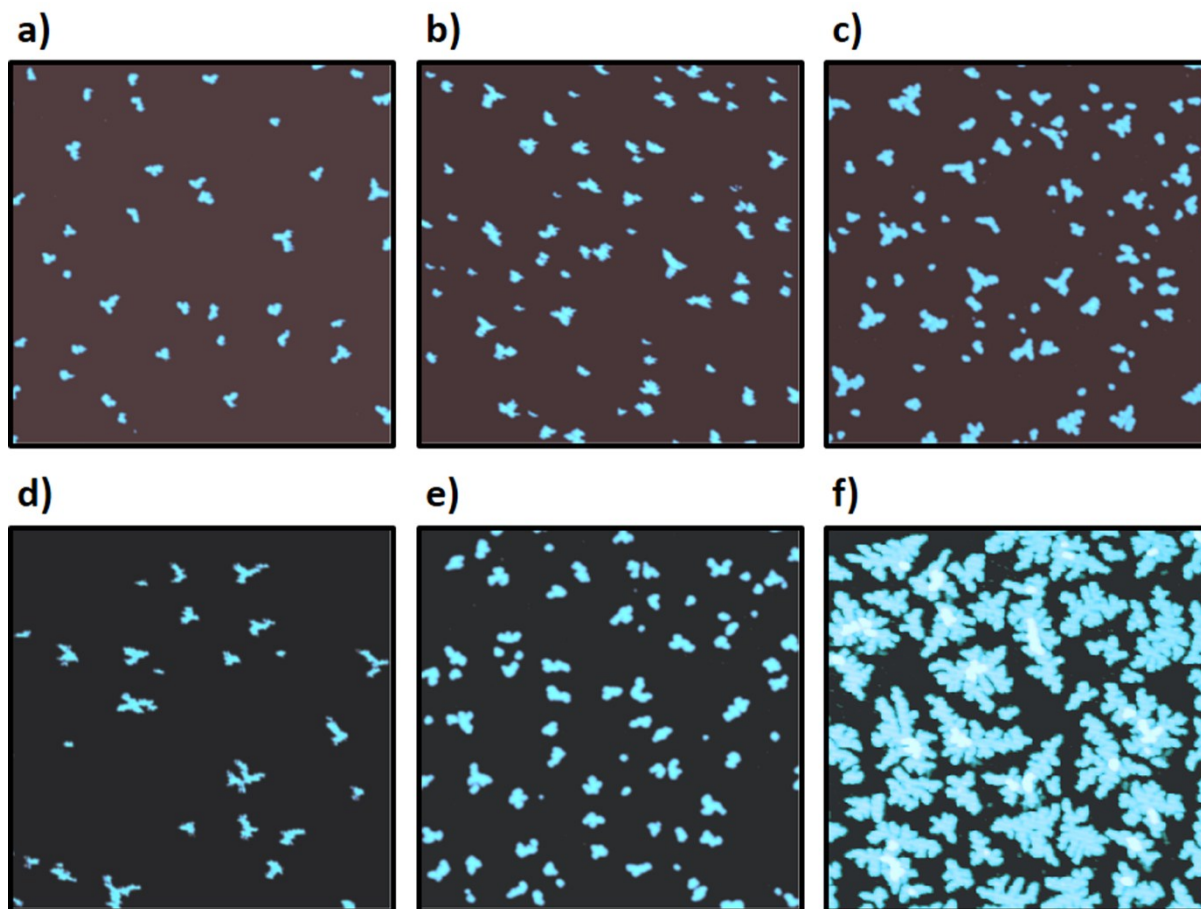


Figure S1. Ir deposition on **a)-c)** Ir(111) and **d)-f)** Rh(111) surfaces at RT. Tunneling parameters: a) $V_s = -1.1$ V, $I_T = 0.38$ nA, b) $V_s = -1.5$ V, $I_T = 0.4$ nA, c) $V_s = -0.4$ V, $I_T = 0.3$ nA, d) $V_s = +1.5$ V, $I_T = 0.5$ nA, e) $V_s = +1.5$ V, $I_T = 0.38$ nA, f) $V_s = +1.5$ V, $I_T = 0.38$ nA. The size of all the images is 100×100 nm².

Auger Spectroscopy characterization of the material

Figure S2 shows a series of AES spectra acquired after each step of sample preparation involved in the growth of the material. Specifically, Figure S2a-d displays AES spectra confirming the absence of Ir on freshly prepared Rh(111) and h-BN/Rh(111) surfaces and its presence after sublimation on them. Figure S2e-g shows AES spectra demonstrating the absence of B and N on

bare Rh(111) surfaces prepared as described in the main manuscript and their presence after the growth of h-BN by thermal decomposition of borazine on the metal support.

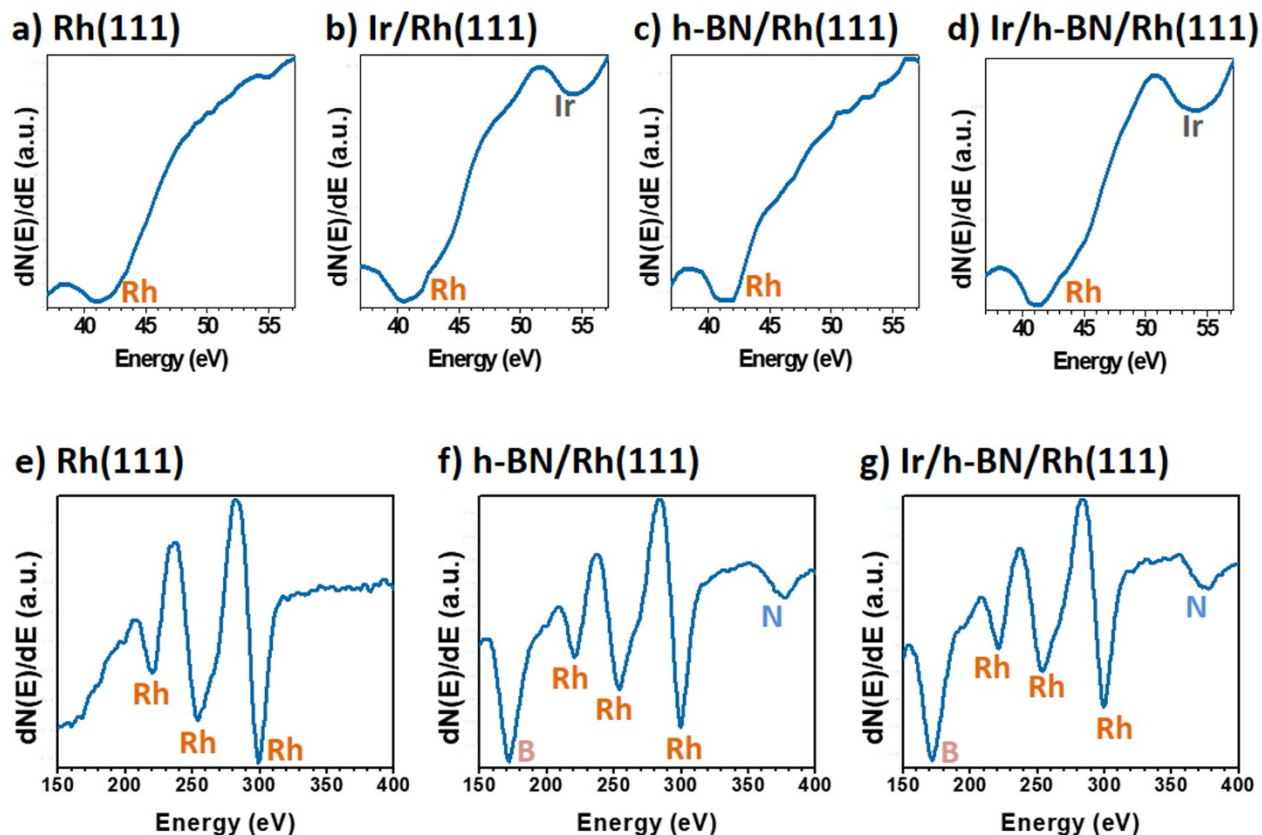


Figure S2. AES analysis of the growth of the material. The energy of the primary electron beam was 2.8 keV.

Structural properties of the material as a function of the amount of Ir

As discussed in the main manuscript, the structure of the material presented here is highly dependent on the amount of Ir deposited over the h-BN/Rh(111) interface. Figure S3 shows additional analysis of the influence of the Ir coverage on the size (lower panels) and spatial distributions (upper panels) of the nanoparticles on the h-BN/Rh(111) template.

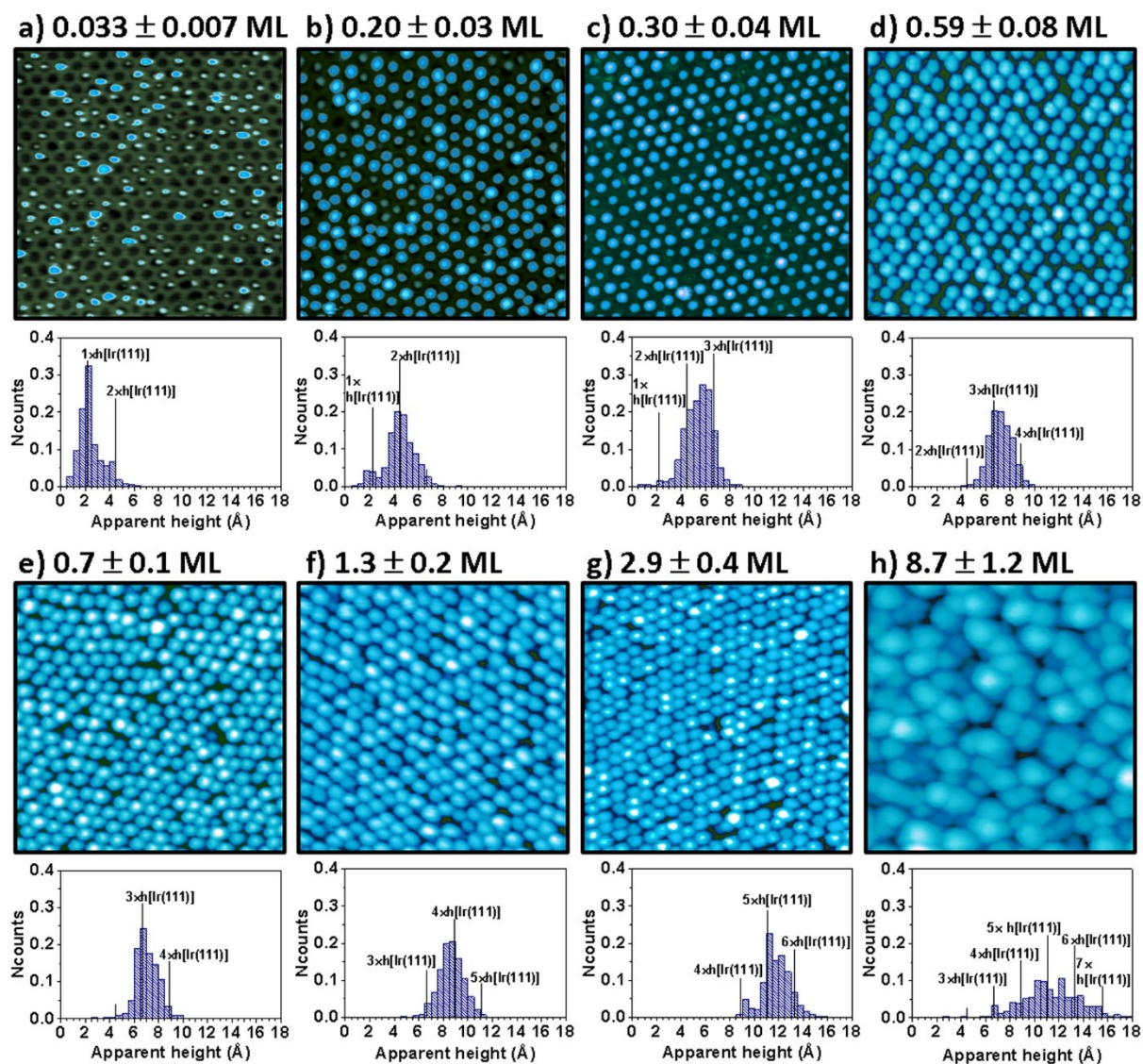


Figure S3. Influence of the Ir coverage on the structure of the material. **a)-h)** Upper panels: Representative STM images illustrating the evolution of the spatial distribution of the nanoparticles with increasing the amount of Ir deposited on the h-BN/Rh(111) template. Tunneling parameters: a) $V_s = +2.2$ V, $I_T = 0.34$ nA, b) $V_s = +2.2$ V, $I_T = 0.4$ nA, c) $V_s = +2.2$ V, $I_T = 0.4$ nA, d) $V_s = +2.2$ V, $I_T = 0.4$ nA, e) $V_s = +2.2$ V, $I_T = 0.4$ nA, f) $V_s = +2.4$ V, $I_T = 0.4$ nA, g) $V_s = +2.2$ V, $I_T = 0.4$ nA, h) $V_s = +2.2$ V, $I_T = 0.2$ nA. The size of all the images is 50×50 nm². Lower panels: Apparent height histograms extracted from a number of STM topographs acquired at each coverage.

The changes in the spatial distribution of the nanoparticles with increasing the amount of Ir deposited can be quantified in terms of the density of these quasi-zero dimensional elements over the h-BN/Rh(111) template. Specifically, as shown in Figure S4, this quantification can be performed directly by means of the average number of nanoparticles per moiré cell n , thereafter occupation number. It is observed that for coverages lower than 0.2 ML, the occupation number increases fairly linear with coverage. Likewise, for coverages in the range 0.2-1.8 ML, n is rather constant and around one, indicating that almost all the nanomesh pores are occupied by nanoparticles. This broad coverage range allows to obtain, by fine-tuning the amount of Ir, different apparent height distributions for the nanoparticles, in the range from two to five times the distance between (111) atomic planes of bulk Ir, with an occupation of roughly 100 % of the nanomesh pores. Finally, for coverages higher than 1.8 ML, the occupation number starts to decrease due to coalescence.

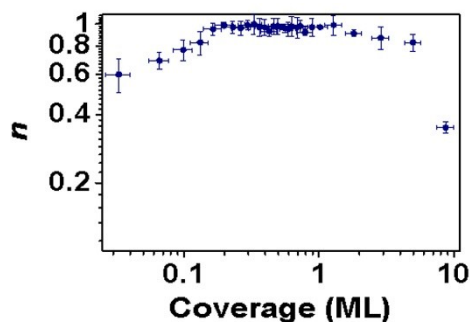


Figure S4. Evolution of the average number of nanoparticles per moiré cell n with increasing the amount of Ir deposited on the h-BN/Rh(111) surface.

As discussed in the main text, nanoparticle positioning does not follow a perfect hexagonal pattern, but there are small deviations associated to the different possibilities for clusters adsorption within the pores. Figure S5 provides additional data of the quantification of these deviations as a function of the Ir coverage by means of first neighbors distances histograms.

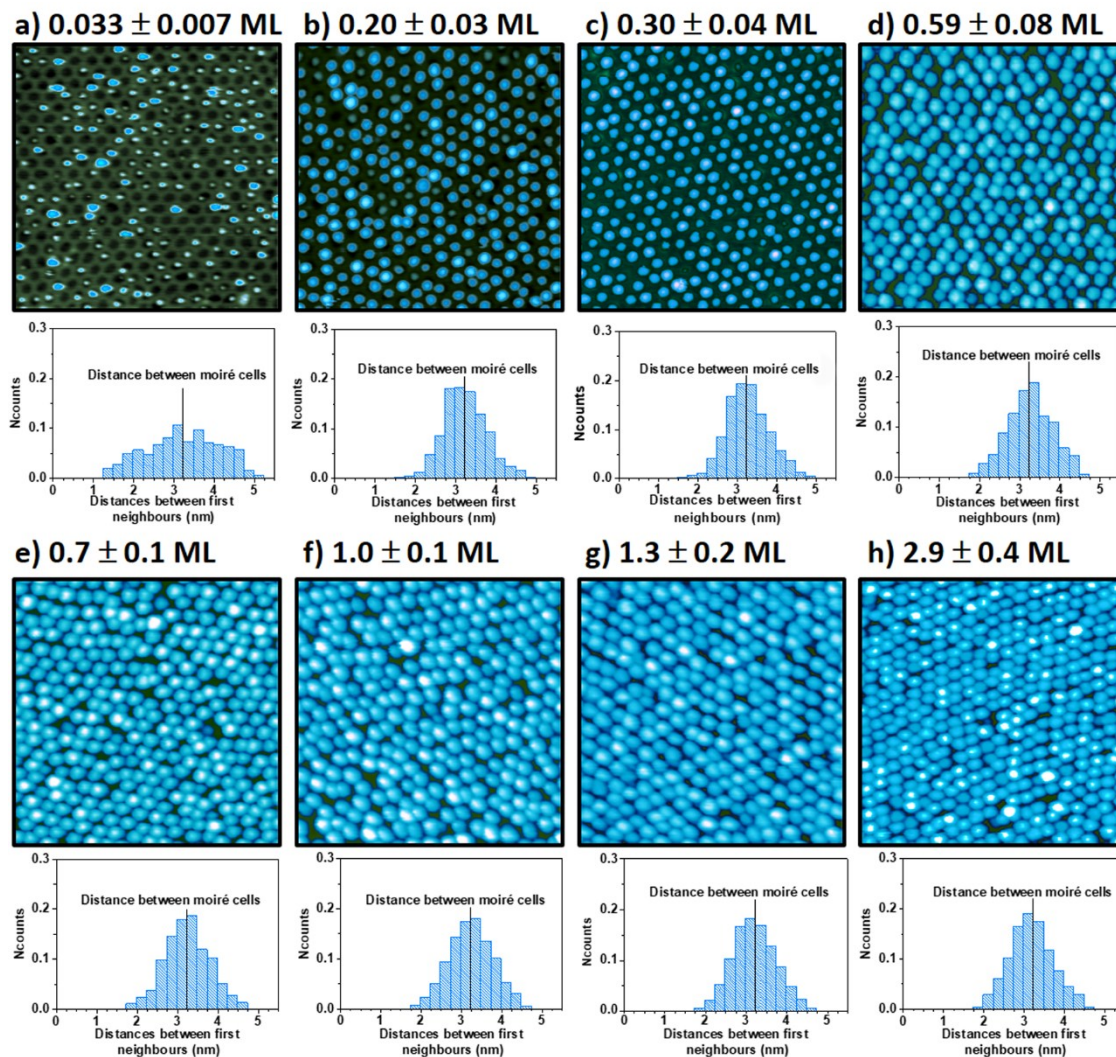


Figure S5. Quantification of the deviations of nanoparticle positioning with respect to a perfect hexagonal superlattice with the periodicity of the nanomesh (i.e., the distance between adjacent moiré cells) resulting on the h-BN/Rh(111) interface. **a)-h)** Upper panels: STM images obtained at various Ir coverages. Tunneling parameters: a) $V_s = +2.2$ V, $I_T = 0.34$ nA, b) $V_s = +2.2$ V, $I_T = 0.4$ nA, c) $V_s = +2.2$ V, $I_T = 0.4$ nA, d) $V_s = +2.2$ V, $I_T = 0.4$ nA, e) $V_s = +2.2$ V, $I_T = 0.4$ nA, f) $V_s = +2.4$ V, $I_T = 0.4$ nA, g) $V_s = +2.4$ V, $I_T = 0.4$ nA, h) $V_s = +2.2$ V, $I_T = 0.4$ nA. The size of all the images is 50×50 nm². Lower panels: Histograms of distances between first neighbor nanoparticles. Each one has been extracted from a number of STM images acquired after depositing, on the h-BN/Rh(111) surface, the amount of Ir indicated on the its upper panel.

Effects of annealing on the structural properties of the material

The effects of annealing on the size and the shape of the nanoparticles, as evidenced in apparent height histograms, as well as those on the deviations of cluster positioning with respect to a perfect hexagonal lattice, observed in first neighbors distances histograms, have been discussed in the main manuscript. Figure S6 and S7 show additional details of those effects along the complete annealing sequence between RT and 970 K discussed in Figure 3 of the main manuscript.

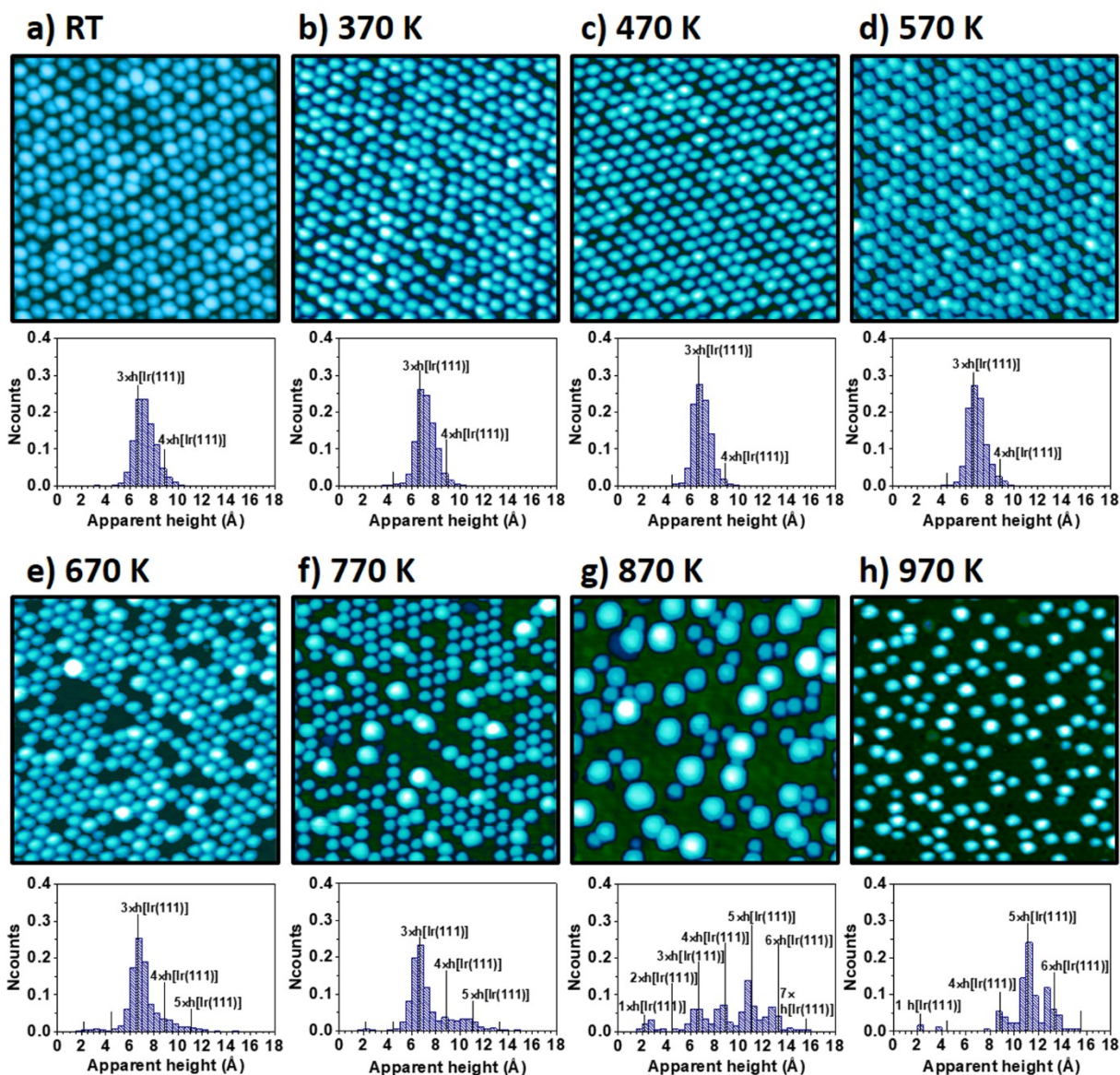


Figure S6. Evolution of nanoparticle size, shape and spatial distribution along annealing. **a-h)** Upper panels: Representative STM images obtained along sequential annealing steps of 300 s at increasing temperatures in intervals of 100 K between RT and 970 K. Tunneling parameters: $V_s = +2.2$ V, $I_T = 0.4$ nA; size: 50×50 nm² for all the topographs. Lower panels: Apparent height histograms obtained from STM images acquired after each annealing step.

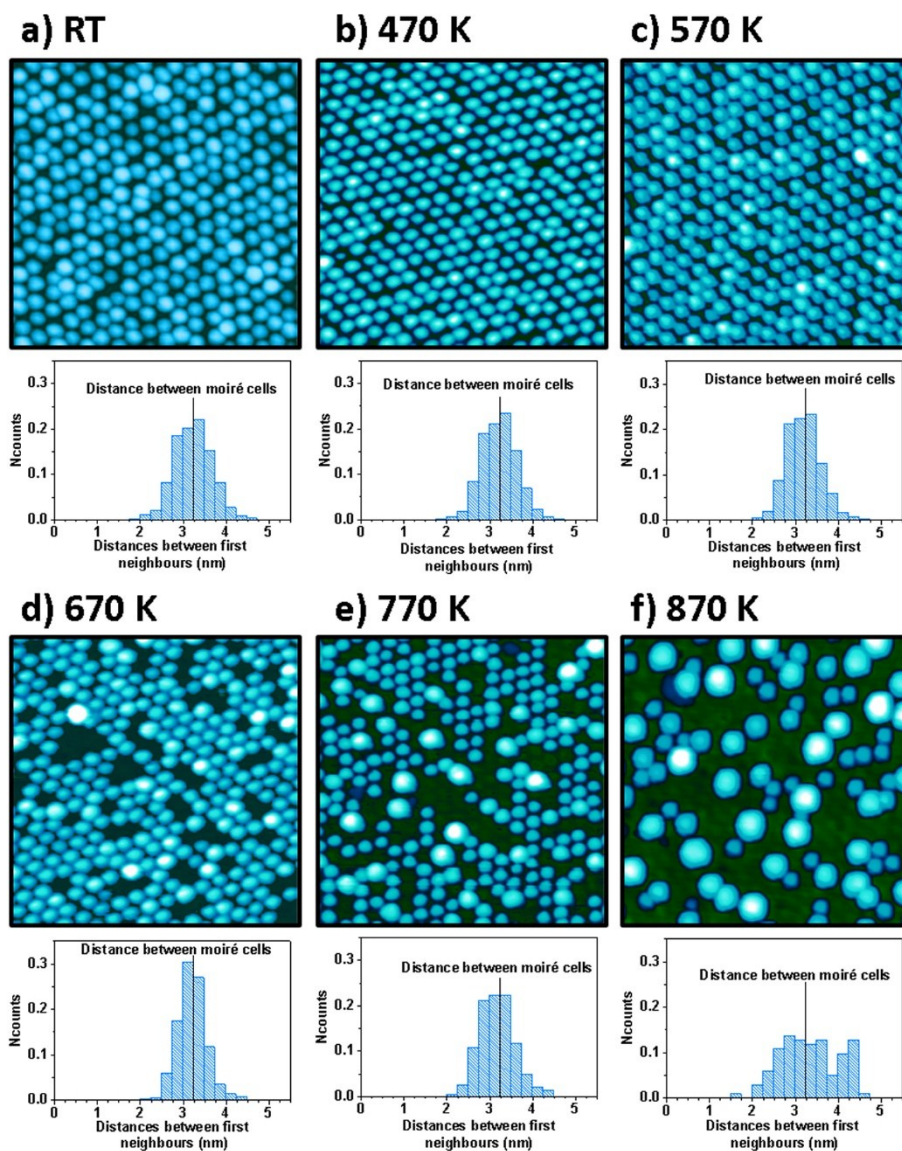


Figure S7. Evolution of the deviations of nanoparticle positioning with respect to a perfect hexagonal lattice with increasing the annealing temperature. **a)-f)** Upper panels: STM images acquired along 300 s stepwise annealing between RT and 970 K in increments of 100 K. Lower panels: Histograms of first neighbors distances extracted from STM topographs obtained after the annealing step corresponding to the temperature indicated in the upper panel. Tunneling parameters: $V_s = +2.2$ V, $I_T = 0.4$ nA; size: 50×50 nm² for all the topographs.

Effects of extended defects in the Rh(111) support on the structural properties of the material

Extended defects, as monatomic steps in the Rh(111) substrate, do not seem to induce strong distortions in the spatial distribution of the nanoparticles (see Figure S8).

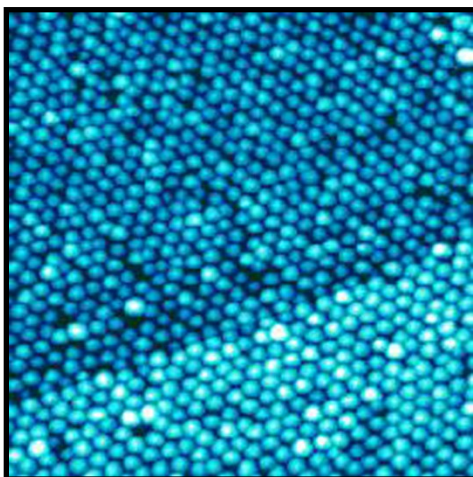


Figure S8. Representative STM image acquired on the material presented here in the surroundings of a monatomic step in the underlying Rh(111) support. Tunneling parameters: $V_s = +2.2$ V, $I_T = 0.38$ nA; size: 80×80 nm².